Novel 14,21-dihydroxy-docosahexaenoic acids: structures, formation pathways, and enhancement of wound healing

Yan Lu, Haibin Tian, and Song Hong[1]

Center of Neuroscience Excellence, Health Science Center, Louisiana State University, New Orleans, LA 70112

Abstract Chronic wounds remain a medical challenge, where well-coordinated cellular and molecular processes required by optimal healing are impaired by diabetes, aging, or other diseases. In determining mechanisms that regulate wound healing, we found that wounding induced formation of novel endogenous 14*S*,21*S*-dihydroxy-docosa-4*Z*,7*Z*,10*Z*,12*E*,16*Z*,19*Z*-hexaenoic acids (14*S*,21*S*-diHDHA);14*R*,21*R*-diHDHA; 14*S*,21*R*-diHDHA; and/or 14*R*,21*S*-diHDHA. 12-lipoxygenase and cytochrome P450 catalysis in tandem converted docosahexaenoic acid to 14*S*,21*R*-diHDHA and 14*S*,21*S*-diHDHA through the intermediacy of 14*S*-HDHA; P450 also converted 14*R*-HDHA to novel 14*R*,21*R*-diHDHA and 14*R*,21*S*-diHDHA. Macrophages function as the combination of 12-lipoxgenase and P450 to generate these 14,21-diHDHA stereoisomers, as well as their intermediates 14*S*-HDHA, 14*R*-HDHA, and 21-HDHA. The structure and formation pathways of 14,21-diHDHA stereoisomers were further confirmed by macrophage biosynthesis of 14,21-diHDHA-21,22,22,22-d_4 stereoisomers, 14*S*-HDHA-d_5, 14*R*-HDHA-d_5, and 21-HDHA-d_4 from DHA-21,21,22,22,22-d_5. We found that 14*S*,21-diHDHA and 14*R*,21-diHDHA enhanced wound closure, reepithelialization, granulation tissue growth, and capillary vasculature formation of murine wounds. 14*S*,21-diHDHA and 14*R*,21-diHDHA produced by macrophages may partially represent the molecular mechanisms for macrophage pro-healing function. Taken together, 14,21-dihydroxy-DHA stereoisomers and their formation pathways may represent a novel mechanism in the orchestration of wound healing processes, which may provide new insight for developing novel therapeutic modalities that counteract impairments to wound healing.—Lu, Y., H. Tian, and S. Hong. **Novel 14,21-dihydroxy-docosahexaenoic acids: structures, formation pathways, and enhancement of wound healing. *J. Lipid Res.* 2010.** 51: **923–932.**

Supplementary key words 14*S*,21*S*-dihydroxy-docosa-4*Z*,7*Z*,10*Z*,12*E*,-16*Z*,19*Z*-hexaenoic acid (14*S*,21*S*-diHDHA) • 14*S*,21*R*-diHDHA, 14*R*,21*S*-diHDHA • 14*R*,21*R*-diHDHA • 14,21-diHDHAs-d_4 • 14-HDHAs-d_5; 21-HDHA-d_4 • reepithelialization • granulation tissue growth • macrophages • vascularization

Successful cutaneous wound healing needs well-coordinated, complex cellular and molecular processes, which include inflammation, cell migration, proliferation, angiogenesis, granulation tissue formation, extracellular matrix deposition, and remodeling (1, 2). Formation of new blood vessels is paramount for optimal healing (1, 2). Impairment of any of these events may lead to chronic wounds, which often occur in diabetic and elderly patients (1, 2). Revealing the molecular mechanisms of these processes may provide novel targets for the development of effective therapies that counteract impairments to wound healing.

Macrophages (Mfs), mostly transformed from recruited blood monocytes, take residence, and then play a major role in clearing the wound of debris (1, 2). Mfs also protect wounds from infection. Furthermore Mfs are capable of efficiently transforming docosahexaenoic acid (DHA) to pro-resolution lipid mediator resolvins, neuroprotectins/protectins, and maresins (3–7). Neuroprotectin D1/protectin D1, a 15-lipoxygenase (LOX) product of DHA (6, 7), was found to occur in and enhance corneal wound healing (8).

Our lipidomic analysis indicates that DHA is a relatively abundant endogenous fatty acid existing in murine skin (in full thickness) (300–3000 ng/g skin tissue). Gel-controlled release of DHA and other ω3 essential fatty acids to wounds significantly promotes wound healing (9), implying potential therapeutic roles for DHA derivatives in

Abbreviations: DHA, docosahexaenoic acid; 14*S* (or *R*)-HDHA, 14*S* (or *R*)-hydroxy DHA; 14-HpDHA, 14-hydroperoxy-DHA ; 14*S* (or *R*),21*S* (or *R*)-diHDHA, 14*S* (or *R*),21*S* (or *R*)-dihydroxy-docosa-4*Z*,7*Z*,10*Z*,12*E*,16*Z*,19*Z*-hexaenoic acid; 14,21-diHDHA-d_4, 14,21-dihydroxy-21,22,22,22-d_4-docosa-4*Z*,7*Z*,10*Z*,12*E*,16*Z*,19*Z*-hexaenoic acid; 21*S* (or *R*)-HDHA, 21*S* (or *R*)-hydroxy-DHA; 21*S* (or *R*)-HDHA-d_4, 21*S* (or *R*)-hydroxy-DHA-d_4; LOX, lipoxygenase; Mfs, macrophages; h-P450, human cytochrome P450.

[1]To whom correspondence should be addressed.
e-mail: shong@lsuhsc.edu

This work was supported by a startup fund from the Center of Neuroscience Excellence, Health Science Center, Louisiana State University (S.H.).

Manuscript received 13 October 2009 and in revised form 30 October 2009

Published, JLR Papers in Press, October 30, 2009
DOI 10.1194/jlr.M000059

wound healing. Some lipid mediators generated by cytochrome P450 (CYP) and 12-lipoxygenase in certain conditions were known to be angiogenic (10, 11). Moreover, skin and Mfs are the major source of 12-LOX and P450 (11–16). Based on this knowledge, we hypothesized that pro-healing lipid mediators are generated from DHA by 12-LOX- and P450-like catalytic actions in tandem in wounds and Mfs. To test this hypothesis, we conducted a targeted mass spectrometry–based lipidomic study, which is an indispensable approach to unravel the molecular structures and quantities of low-abundant bioactive lipid molecular species during wound healing (17). We used the well-accepted splinted excisional wound murine model, where the splints prevent skin contraction and allow wounds to heal through reepithelialization and granulation. Healing of these wounds is accurate and reproducible and closely resembles wound healing in humans (18–20). We also studied biosynthesis of novel pro-healing mediators in Mfs. From these studies, we found novel DHA-derived ω-1-hydroxy docosanoids in wounds and Mfs. Moreover, we found that these novel docosanoids promote wound healing and microvasculature formation. Here we report these findings.

MATERIALS AND METHODS

Reagents

DHA, DHA-21,21,22,22,22-d_5 (DHA-d_5), 14*S*/*R*-hydroxy DHAs (14*S*/*R*-HDHAs) (racemic), and porcine leukocyte (L)-12-LOX were purchased from Cayman (Ann Arbor, MI). Interleukin (IL)-1β, TNF-α, and *Escherichia coli* lipopolysaccharide (LPS) were supplied by Sigma (St. Louis, MO).

Murine splinted excisional wound healing model

The published protocols were followed (18–20), and studies were conducted in blinded fashions and in conformity with the Public Health Service Policy on Humane Care and Use of Laboratory Animals. Animal protocols and all such investigations were approved by the Institutional Animal Care and Use Committee and Institutional Review Board of Louisiana State University Health Sciences Center, New Orleans; and followed the National Institutes of Health guidelines for experimental animal use. Briefly, under sterile conditions and anesthesia, paired 4-mm circular, full-thickness wounds symmetrically along the midline were made on the dorsal skin of the mice (~22 g body weight, Balb/c, female, 8–10 weeks old). For each of two wounds on a mouse, PBS with specific docosanoids (50 ng) was applied to the wound-bed (10 μl) and injected intradermally to 4 points (10 μl/site) evenly distributed near the wound edge (50 μl total). A donut-shaped 0.5 mm-thick silicone splint was concentric with a wound and fixed to the skin surrounding the wound with an immediate-bonding adhesive (Krazy Glue®) and 6–0 nylon sutures; and then a transparent sterile occlusive dressing then was placed over the wound and the splint (20). Mice were fed with a standard chow diet Teklad 2018 containing 0% DHA and 2.76% ω3 α-linolenic acid of total fatty acids (21). α-linolenic acid can be converted to DHA in rodents (22).

Analysis of wound healing

Wound closure was quantified as relative reduction of the initial wound area by analyzing wound digital-photographs taken at day 0, 3, 7, 10, and 14 postwounding (18). For immunohistological study, mice were sacrificed at day 4 postwounding. Wounds with a 2 mm margin of normal surrounding skin were excised, fixed in 4% paraformaldehyde (4 h), incubated in 30% sucrose (12 h), and embedded in OCT. Serial cryosections (10 μm thick/section) were made, stained with rat anti-mouse CD31 antibody (Santa Cruz Biotech, Santa Cruz, CA) (18, 19) and then with secondary PE-goat anti-rat IgG (red); nuclei were stained with Hoechst 33342 (blue). The capillary vascular density in the wound bed was determined as CD31+ cells in wound bed/microscope field by examining three fields per section of the wound between the edges in six successive sections. The other wound cryosections were stained with hematoxylin-eosin, then analyzed by microscopy (18). Sections representing the widest wound beds were chosen to determine granulation tissue area and epithelial gap (distance between leading epithelial edges, measured from wound edges), both of which were measured in pixels. For comparison of different treatments of wounds, capillary vascular density, granulation tissue area, and epithelial gap were presented as relative percentages after normalized to the values of corresponding PBS control. NIH Image J1.40 programs were used for the analysis (NIH, Bethesda, MD) (18).

LC-UV-MS/MS analysis of docosanoids

We conducted this analysis in the same manner as in earlier studies (6, 23). In brief, we used a liquid chromatography-photodiode array ultra-violet detector-LTQ linear ion trap mass spectrometer (LC-UV-MS/MS) (Thermo, Waltham, MA) equipped with a chiral column (AD-RH, 150 mm × 2.1 mm × 5 μm) (Chiral Tech, West Chester, PA) (24). Both wideband activation and non-wideband activation were used for MS/MS. The wideband activation excites and fragments ions with mass-to-charge ratio between M and M - 20, which generates higher abundance of ions from cleavage of the carbon chain, and provides more structure information of the analytes. The mobile phase flowed at 0.15 ml/min; it eluted as D (acetonitrile:H_2O:acetic acid = 45:55:0.01) from 0 to 45 min, ramped to acetonitrile from 45.1 to 60 min, flowed as acetonitrile for 10 min, and then ran as D again for 10 min. DHA-d_5 (50ng) was used as internal standard, except for the incubations using DHA-d_5 as substrate. Murine skin tissues were extracted with ice-cold acetonitrile three times through homogenization and sonication. Incubations of cells were adjusted to pH 5.5 by adding HCl (1 M) (on ice), and three volumes of ice-cold acetonitrile were added into each sample (sample: acetonitrile = 1: 3 by volume). Each mixture was vortexed well, then sonicated in water bath (4°C). After centrifugation (3000 rpm, 15 min, 0°C), each pellet was extracted again with three volumes of acetonitrile (pellet: acetonitrile = 1: 3) twice. The supernatants for each sample were pooled together and adjusted to the content of 10% acetonitrile by adding water, and then cleaned up via C18 solid-phase extraction (500 mg, Varian, Palo Alto, CA). The final extracts were reconstituted into acetonitrile for lipidomic analysis.

Enzymatic formation of novel ω-1-hydroxy docosanoids

14*S*,21-dihydroxy-docosa-4*Z*,7*Z*,10*Z*,12*E*,16*Z*,19*Z*-hexaenoic acids (14*S*,21-diHDHAs) were formed as follows. First the intermediate 14*S*-hydroxy-DHA (14*S*-HDHA) was generated by incubating DHA (50 μg) with porcine leukocyte-12-LOX (L-12-LOX) (1000 unit) (Cayman) in 0.1 M tris buffer (pH 7.4) containing 0.01% Triton-114 (Sigma) (37°C, 20 min) followed by reduction by $NaBH_4$.

The incubation was extracted by ethyl acetate three times after its pH was adjusted to 3.5. 14*S*-HDHA was isolated from the extract using chiral LC as described above. Additionally 14*S*-HDHA

and 14*R*-HDHA were prepared from racemic 14*S*/*R*-HDHAs (Cayman) using the same chiral LC-UV-MS/MS conditions. 14*S*,21-diHDHAs, 14*R*,21-diHDHAs, and 14*S*/*R*,21-diHDHAs were prepared by incubation of 14*S*-HDHA, 14*R*-HDHA, and 14*S*/*R*-HDHAs (10 μg/each), respectively, with a human cytochrome P450 (h-P450) enzyme mixture (BioCatalytics Inc., Pasadena, CA) (30°C, 12 h). The h-P450 mixture contained NADPH cofactor, buffer salts, and 1 nmol of seven h-P450 in fixed ratios (recombinant human CYP1A2, 2C8, 2C9, 2D6, 2E1, and 3A4). One of the objectives for this paper was to determine if any P450 could participate in 14,21-diHDHA formation from DHA as well as intermediates 21-HDHA, 14*S*-HDHA, and 14*R*-HDHA. However, determining exactly which P450s are responsible for 14,21-diHDHA formation was beyond the scope of this paper. Therefore, we used a mixture of P450s.

Biosynthesis of ω-1-hydroxy docosanoids and intermediates by Mfs

Thioglycollate-induced Mfs were collected by lavage from murine peritoneal cavity (peritoneal exudate cells, PECs) 3 days after injecting 2.5 ml of 4% thioglucoate (i.p.) as in (25). PECs were washed and cultured (24 h, 37°C, 5% CO_2) in RPMI1640 containing 10% FBS and other components (25). Plates were washed three times with culture medium to remove nonadherent cells. Then adherent cells were harvested, of which more than 90% were F4/80$^+$.

To generate 14*S*,21-diHDHAs, 14*R*,21-diHDHAs, and/or their deuterated isotopomers, Mfs purified above (5×10^6 cells) were cultured in PBS containing DHA, 14*S*-HDHA, 14*R*-HDHA, or DHA-d_5 (1 μM) for 20 min, then stimulated at 37°C for 1 h with TNF-α (10 ng/ml), IL-1β (10 ng/ml), and LPS (100 ng/ml). DHA in full thickness murine skin wounds can reach as high as 1-9 μmol/kg level (data not shown). Thus 1 μM of docosanoic substrate is within concentration range in physiopathological condition of skin. Stimulation with TNF-α and IL-1β mimics the environment of tissue injury, while LPS treatment resembles infection potential during wound healing (26). Adding TNF-α, IL-1β, and LPS to macrophages promotes the expression of phospholipase A2 that releases polyunsaturated fatty acids from membranes and/or other parts of the cells; it is also likely to enhance 12/15 lipoxygenase-like activity (26) that results in 14-hydroxylation of DHA and some DHA derivatives (27). The cells and medium from each culture were extracted for the analysis and preparation as described in "LC-UV-MS/MS analysis of docosanoids" for 14,21-diHDHAs or their biosynthetic intermediates.

Statistical analysis

Results were reported as mean ± SEM and analyzed with 2-way ANOVA with a posthoc test. Accepted level of significance for all tests was $p < 0.05$.

RESULTS

Wounding prompts formation of novel endogenous 14,21-diHDHAs

Three peaks (I, II, and III) of novel DHA-derived 14,21-dihydroxy-docosa-4*Z*,7*Z*,10*Z*,12*E*,16*Z*,19*Z*-hexaenoic acids were found using chiral LC-UV-wideband activation MS/MS analysis of wounded skin tissues from mice after splinted excisional wounding. They were much less in unwounded skin tissues, indicating wounding induced their formation (**Fig. 1A** and 1B, top). The chiral LC-MS/MS spectra of three peaks of endogenous 14,21-diHDHAs in wounds, shown in selective ion chromatogram of *m/z* 271 in MS/MS at *m/z* 359, have identical ions with similar or different relative abundance. Each spectrum acquired with wideband activation (Fig. 1A) possessed ions at *m/z* 359 [M-H]$^-$, 323 [M-H-2H_2O]$^-$, 297 [M-H-CO_2-H_2O]$^-$, 279 [M-H-CO_2-2H_2O]$^-$ that were consistent with its molecular weight (M) 360, one carboxy (for loss of CO_2), and two hydroxys (for loss of two H_2O); ions *m/z* 205, 161 [205-CO_2]$^-$, 233, and 189 [233-CO_2]$^-$, demonstrated a hydroxy at its 14 position; and ion *m/z* 315, generated from cleavage of the C_{20}-C_{21} bond, as well as ion *m/z* 271 [315-CO_2]$^-$ and 253 [315-CO_2-H_2O]$^-$ showed another hydroxy at the C_{21} position (Fig. 1A). The wideband activation energizes ions between *m/z* [M-H] to [M-H-20], which generated more intensive diagnostic ions from the cleavage of [M-H] carbon-chain (28) and nearly completely diminished the signal of ion *m/z* 341 [M-H-H_2O]. The ions *m/z* 189 and 233 from MS/MS 359 under non-wideband activation have low abundances which bring uncertainty to the identification of 14-OH (data not shown), with wideband activation, these two ions are much more abundant and reduce the uncertainty (Fig. 1A).

Enzymatic formation and pathways of 14*S*,21-diHDHAs and 14*R*,21-diHDHAs

14*S*,21-diHDHAs and 14*R*,21-diHDHAs were investigated for the elucidation of their chemical structures and formation pathways. Incubation of DHA with porcine L-12-LOX produced 14*S*-hydroperoxy-DHA (HpDHA), which was reduced by $NaBH_4$ to 14*S*-HDHA. Chiral LC was used to isolate 14*S*-HDHA (Fig. 1C, middle) from the incubations, as well as 14*R*-HDHA and 14*S*-HDHA from racemic 14*S*/*R*-HDHA (Fig. 1C, bottom), where the *R*-hydroxy-DHA (e.g., 14*R*-HDHA) has shorter retention time (RT) than its *S*-hydroxy stereoisomer (14*S*-HDHA) (Fig. 1C, middle and bottom). The order that *R*-hydroxy compound is eluted before its *S*-epiomer using this kind chiral LC also fits to other hydroxy DHA (data not shown), except 21-HDHA which seems not to be separable. It also fits to hydroxy eicosatetraenoic acids (24). Additionally, $PGF_{2\alpha}$ (with 15*S*-hydroxy) is reported eluted after 15*R*-hydroxy $PGF_{2\alpha}$ (29). P450 hydroxylated 14*S*-HDHA to two 14*S*,21-diHDHAs which were separated by the chiral LC (Fig. 1B, upper middle). The C_{14} chiral configuration and double-bond geometry of 14-HDHA are expected to be conserved when 14-HDHA is converted by P450 to 14,21-diHDHAs based on the established knowledge that ω-1-oxidation does not change the chirality and double-bond configurations on other carbon positions of eicosanoid substrates (30, 31). Therefore the configurations (*R* and *S*) of asymmetric C_{21} in 14*S*,21-diHDHAs are responsible for two isomers observed (Fig. 1B, upper middle), which were assigned as 14*S*,21*R*-diHDHA and 14*S*,21*S*-diHDHA for the chiral LC peaks from left to right. For similar reasons, two 14*R*,21-diHDHAs generated from 14*R*-HDHA by h-P450 are 14*R*,21*R*-diHDHA and 14*R*,21*S*-diHDHA which are separated as two chiral LC peaks from left to right (Fig.1B, lower middle). LC peak areas of 14*R*,21*R*-,

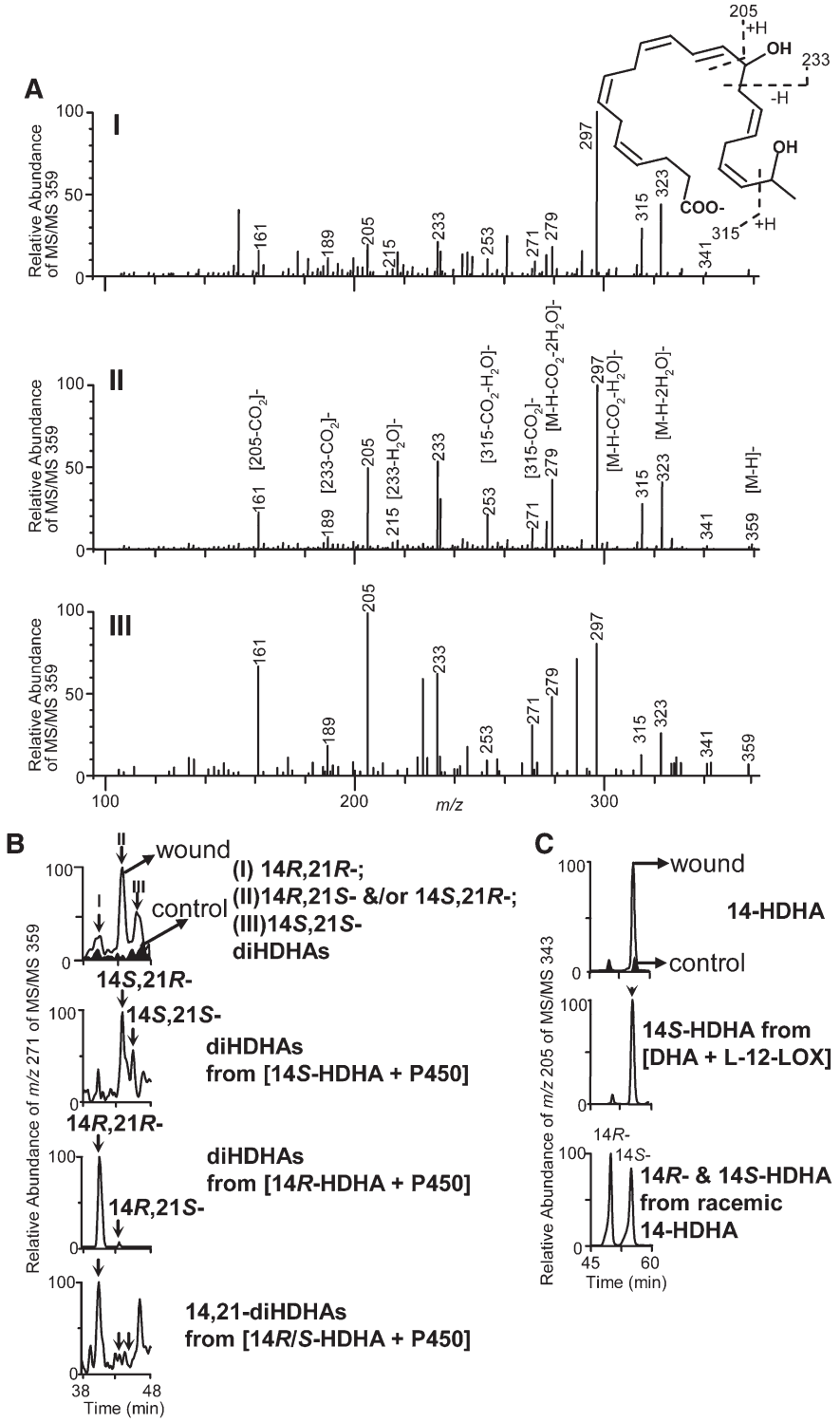

14*R*,21*S*- and/or 14*S*,21*R*-, and 14*S*,21*S*-diHDHA generated from racemic 14-HDHAs (*S*:*R* 1:1) by h-P450 are in the ratio of 23:1:1.6 (Fig. 1B, bottom), suggesting that 14*R*-HDHA is better substrate than 14*S*-HDHA to be converted by the h-P450 to 14,21-diHDHAs.

Peaks I, II, III acquired from wound skin were identified as 14*R*,21*R*-diHDHA, 14*S*,21*R*-diHDHA/14*R*,21*S*-diHDHA, and 14*S*,21*S*-diHDHA, respectively, because each of their chiral LC-UV-MS/MS spectra and chromatographic RTs matches to that of the counterpart generated from enzyme incubations (Fig. 1A, B). 14*S*,21*R*-diHDHA had just slightly longer RT than 14*R*,21*S*-diHDHA (Fig. 1B, upper and lower middle), they were not distinguishable by chiral LC RT. The main mono-hydroxy-DHA in wounds was found to be 14*S*-HDHA, the precursor of 14*S*,21-diHDHAs, of which the chiral LC-UV-MS/MS spectrum matches that of 14-HDHA (32), and the chiral LC retention time (Fig. 1C, top) matches that of 14*S*-HDHA obtained from incubation of DHA with L-12-LOX (Fig. 1C, middle) or from racemic 14*S*/*R*-HDHA standard (Fig. 1C, bottom). 14*R*-HDHA in wounds was much less than 14*S*-HDHA. The formation of 14*S*-HDHA was induced by wounding because the chiral LC peak of 14*S*-HDHA in wounds was much higher than that from the nonwounding control (Fig. 1C, top). This is consistent with studies showing that 12-LOX activity transforms DHA to 14*S*-HDHA (33–35). The approximate ratio of 14,21-diHDHA to 14-HDHA in wounds is about 1:7 based on the LC-MS peak areas in selective ion chromatograms at *m/z* 359 and *m/z* 343, respectively. The strong UV background from samples in the LC-UV-MS/MS analysis made it impossible to calculate the relative ratio from the absorbance at ~235 nm. 21-HDHA reported in 1984 (36) was also found in wounds (Fig. 1D), The MS/MS ions *m/z* 343 $[M\text{-}H]^-$, 325 $[M\text{-}H\text{-}H_2O]^-$, 281$[M\text{-}H\text{-}H_2O\text{-}CO_2]^-$, 299, 255 $[299\text{-}CO_2]^-$ demonstrate its structure. The UV spectrum of 21-HDHA with λ_{max} at 202 is consistent with its structure of nonconjugated double bonds.

Biosynthesis of 14,21-diHDHAs and their intermediates by macrophages

We studied 14,21-diHDHA biosynthesized by Mfs through comparison with 14,21-diHDHAs generated by h-P450 using LC-UV-MS/MS analysis. After stimulation with TNF-α, IL-1β, and LPS, Mfs converted 14*R*-HDHA to 14*R*,21*R*-diHDHA and 14*R*,21*S*-diHDHA (**Fig. 2A**); 14*S*-HDHA to 14*S*,21*R*-diHDHA and 14*S*,21*S*-diHDHA (Fig. 2B); DHA to 14*R*,21*R*-diHDHA, 14*S*,21*R*-diHDHA and/or 14*R*,21*S*-diHDHA, and 14*S*,21*S*-diHDHA (Fig. 2C). Each MS/MS spectrum matches that of the same 14,21-diHDHA stereoisomer generated by h-P450 (Fig. 1B). The corresponding UV spectra also matched to each other with λmax of 235–236 nm representing a pair of conjugated double-bonds in each 14,21-diHDHA stereoisomer (insets of Fig. 2A, B).

The wideband activation generated MS/MS spectra of 14,21-diHDHA stereoisomers have nearly identical MS/MS ions. However the relative abundances for some of their MS/MS ions are quite different (Fig. 2A, B). For example, ion *m/z* 253 from MS/MS 359 of 14*R*,21*S*-diHDHA and 14*S*,21*S*-diHDHA has lower relative abundance than that of 14*R*,21*R*-diHDHA and 14*S*,21*R*-diHDHA. This is reflected in the selective ion chromatograms of *m/z* 253 from MS/MS at *m/z* 359. These chromatograms were so insensitive to 14*R*,21*S*-diHDHA and 14*S*,21*S*-diHDHA that we were not able to show these two stereoismers generated from the incubation [14*S*-HDHA + P450] and [14*R*-HDHA + P450], respectively (data not shown). However, the relative abundances of ion *m/z* 271 from MS/MS at *m/z* 359 (Fig. 2A, B) are different from these of *m/z* 253. We used wideband activation MS/MS and observed four 14,21-diHDHA stereoisomers with selective ion chromatograms of *m/z* 271 from MS/MS at *m/z* 359 (Fig. 1B). We saw all four 14,21-diHDHA stereoisomers because selective ion chromatograms of *m/z* 271 from MS/MS at *m/z* 359 are sensitive enough to reveal the present of 14*R*,21*S*-diHDHA and 14*S*,21*S*-diHDHA (Fig. 1B).

14*R*,21*S*-diHDHA coelutes with 14*S*,21*R*-diHDHA (Fig. 1B, upper and lower middle; Fig. 2A, B) under the chiral LC. It is implicated that the abundance ratio of *m/z* 253/271 is <1 in 14*R*,21*S*-diHDHA MS/MS spectrum (Fig. 2A, right) and is >1 in 14*S*,21*R*-diHDHA MS/MS spectrum (Fig. 2B, middle). This ratio may provide semiqualitative information to find if a 14,21-diHDHA peak at this RT is mainly 14*R*,21*S*- or 14*S*,21*R*-diHDHA although the accurate quantification will need the LC separation of these two stereoisomers. At this stage 14*R*,21*S*- or 14*S*,21*R*-diHDHA is still not separable by LC. Additionally mono-hydroxy DHAs generated by Mfs from DHA are mainly 14*S*-HDHA, as well as 14*R*-HDHA and 21-HDHA in much less amounts (Fig. 2C, middle and right).

Fig. 1. Formation of endogenous 14*S*,21-diHDHAs and 14*R*,21-diHDHAs is induced by wounding: molecular structures and formation pathways. Wound tissues were collected from Balb/c mice 3 d after the splinted excisional wounding was performed (n = 3). A: Three typical spectra of chiral LC-MS/MS chromatographic peaks I, II, and III (see 1B) demonstrate the 14,21-diHDHA structure (inset) where the diagnostic MS/MS ions are illustrated. B: Chiral-LC-MS/MS chromatograms show that wounding induced endogenous 14,21-diHDHAs are 14*R*,21*R*-diHDHA (I), 14*S*,21*R*-diHDHA or 14*R*,21*S*-diDHA (II), and 14*S*,21*S*-diHDHA (III) which were identified through matching their chiral LC-MS/MS chromatograms and spectra to those of P450-generated 14*S*-HDHA-derived 14*S*,21R-diHDHA and 14*S*,21*S*-diHDHA (upper middle) as well as 14*R*-HDHA-derived 14*R*,21*R*-diHDHA and 14*R*,21*S*-diHDHA (lower middle). Bottom panel is the chiral LC-MS/MS chromatogram of 14*R*,21*R*-diHDHA, 14*R*,21*S*-diHDHA and/or 14*S*,21*R*-diHDHA, and 14*S*,21*S*-diHDHA generated by P450 from racemic 14-HDHAs (*S*:*R* 1:1). C: Chiral LC chromatograms show that wounding mainly induced the formation of 14*S*-HDHA (with minor amount of 14*R*-HDHA), the intermediate for 14*S*,21*R*-diHDHA and 14*S*,21*S*-diHDHA biosynthesis. The chirality was identified by the comparison with chiral LC chromatograms of 12-LOX-generated 14*S*-HDHA (middle) as well as 14*R*-HDHA and 14*S*-HDHA of racemic 14-HDHA standard (bottom). D: Chiral LC-MS/MS spectrum endogenous 21-HDHA in wounds, left inset is the structure of 21-HDHA with MS/MS fragmentation interpretation, right inset is the UV spectrum.

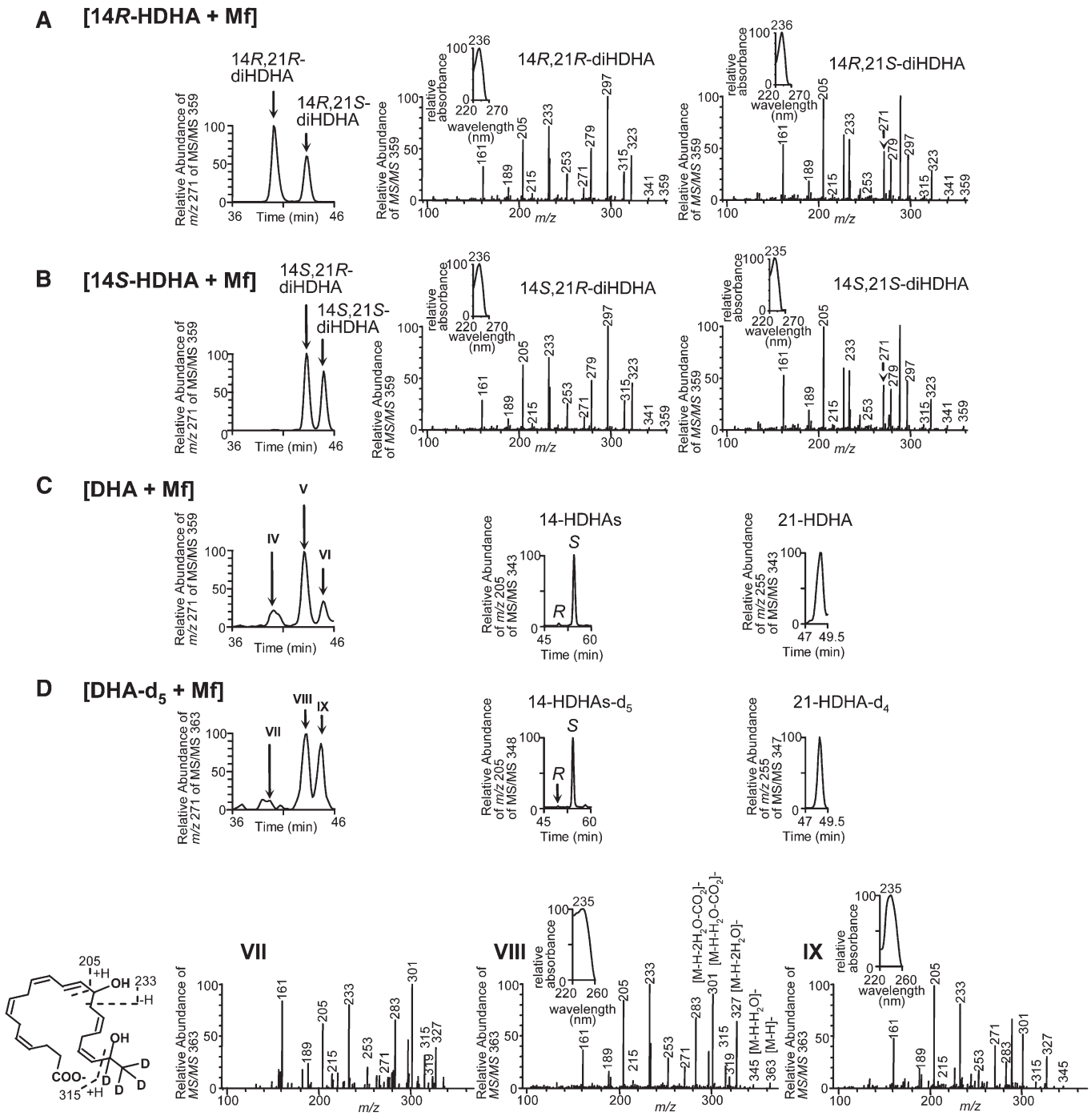

Fig. 2. Macrophages produce 14*S*,21*R*-diHDHA, 14*S*,21*S*-diHDHA, 14*R*,21*R*-diHDHA, 14*R*,21*S*-diHDHA, 14*S*-HDHA, 14*R*-HDHA, and 21-HDHA. Chiral LC-UV-MS/MS chromatograms and/or spectra show that Mfs generated: (A) 14*R*,21*R*-diHDHA and 14*R*,21*S*-diHDHA from 14*R*-HDHA; (B) 14*S*,21*R*-diHDHA and 14*S*,21*S*-diHDHA from 14*S*-HDHA; (C) 14*R*,21*R*-diHDHA (IV), 14*R*,21*S*-diHDHA and/or 14*S*,21*R*-diHDHA (V), 14*S*,21*S*-diHDHA (VI), 14*R*-HDHA, 14*S*-HDHA, and 21-HDHA from DHA; and (D) 14*R*,21*R*-diHDHA-d_4 (VII), 14*R*,21*S*-diHDHA-d_4 and/or 14*S*,21*R*-diHDHA-d_4 (VIII), 14*S*,21*S*-diHDHA-d_4 (IX), 14*R*-HDHA-d_5, 14*S*-HDHA-d_5, and 21-HDHA-d_4 from DHA-d_5. Murine resident peritoneal Mfs (5×10^6 cells) were incubated in PBS containing 14*R*-HDHA, 14*S*-HDHA, DHA, or DHA-d_5 (1 μM) for 20 min, then stimulated for 1 h with TNF-α (10 ng/ml), IL-1β (10 ng/ml), and LPS (100 ng/ml). Mfs and medium from each incubation were extracted and analyzed.

The identification of 14,21-diHDHA structures were confirmed by the LC-UV-MS/MS data of 14,21-diHDHA-d_4 stereoisomers using the same chiral LC-MS/MS with wideband activation (Fig. 2D). Similar to the approaches for 14,21-diHDHA stereoisomers, we used selective ion chromatograms of *m/z* 271 from MS/MS at *m/z* 363 that avoided the insensitivity to 14*R*,21*S*-diHDHA-d_4 and 14*S*,21*S*-diHDHA-d_4, and we observed 3 peaks of 14,21-diHDHA-d_4 stereoiosmers from DHA-d_5. The MS/MS spectrum for each 14,21-diHDHA-d_4 is presented in Fig. 2D.

Mfs converted DHA-d_5 to 14*R*,21*R*-diHDHA-d_4, 14*R*,21*S*-diHDHA-d_4 and/or 14*S*,21*R*-diHDHA-d_4, and 14*S*,21*S*-

diHDHA-d_4, which are identified as chiral LC-MS/MS chromatographic peak (at *m/z* 271 of MS/MS 363) VII, VIII, and IX, respectively (Fig. 2D). Their LC-UV-MS/MS spectra and RTs are consistent with those of corresponding 14,21-diHDHA stereoisomers from wounds (Fig. 1A and 1B, top), h-P450 incubation (Fig. 1B, middle and bottom), or macrophage incubation (Fig. 2A–C); and are in support of the structure elucidation. One deuterium at C_{21} was replaced by 21-hydroxyl and the other 4 deuterium atoms remained, rendering the molecular ion of 14,21-diHDHA-d_4 to be *m/z* 363 (Fig. 2D, lower); MS/MS ions *m/z* 315, 271 [315-CO_2]$^-$ and 253 [315-CO_2-H_2O]$^-$ show a hydroxy at C_{21}; *m/z* 205, 161 [205-CO_2]$^-$, 233, 189 [233-CO_2]$^-$, and 215 [233-H_2O]$^-$ show another hydroxy at C_{14}; and *m/z* 363 [M-H]$^-$, 327 [M-H-2H_2O]$^-$, 301 [M-H-CO_2-H_2O]$^-$, 283 [M-H-CO_2-2H_2O]$^-$ indicate that there are two hydroxys and one carboxy in 14,21-diHDHA-d_4 stereoisomers. The MS/MS spectrum of 14*S*,21-diHDHA-d_4 in Fig. 2D was also acquired using wideband activation of which the ion-trap isolated parent ion (*m/z* 363.2 for 14,21-diHDHA-d_4) along with its fragment ions within *m/z* 363.2 to 343.2 (= 363.2 − 20) were activated. *m/z* 345 [M-H-H_2O] produced by H_2O loss from *m/z* 363.2 of 14,21-diHDHA-d_4 was activated by wideband and efficiently fragmented so that it could barely be seen in the MS/MS spectrum of 14,21-diHDHA-d_4.

Peak VIII (Fig. 2D, upper left and lower middle) is very likely to be mainly 14*S*,21*R*-diHDHA-d_4 because its RT (Fig. 2D, upper left), MS/MS and UV spectra, and abundance ratio (>1) of *m/z* 253/271 in MS/MS spectrum (Fig. 2D, lower middle) is comparable to that for 14*S*,21*R*-diHDHA (Fig. 2B, left and middle). The LC separation of 14*R*,21*S*-diHDHA-d_4 and 14*S*,21*R*-diHDHA-d_4 is needed to quantitatively determine the exact composition of peak VIII. In parallel, LC peak II and V of 14,21-diHDHA from wounds (Fig. 1A, B) and [DHA + Mf] (Fig. 2C, left), respectively, is also likely to be mainly 14*S*,21*R*-diHDHA for the similar reason, and the LC separation of 14*R*,21*S*-diHDHA and 14*S*,21*R*-diHDHA should allow accurate quantification of its composition. Moreover, the mono-hydroxy DHAs-d_5 are 14*S*-HDHA-d_5 (major) with minor amounts of 14*R*-HDHA-d_5 and 21-HDHA-d_4 (Fig. 2D, upper middle and right), similar to the profile of mono-hydroxy DHAs generated by Mfs from DHA (Fig. 2C).

14,21-dihydroxy docosahexaenoic acids promote wound healing

The actions of 14*S*,21-diHDHA and 14*R*,21-diHDHA in wound healing were investigated using murine splinted excisional-wound healing model (**Fig. 3**). When administrated to wounds, 14*R*,21-diHDHA (14*R*,21*R*-diHDHA:14*R*,21*S*-diHDHA10:1) or14*S*,21-diHDHA (14*S*,21*R*-diHDHA:14*S*,21*S*-diHDHA 2:1) significantly accelerated wound closure at day 7 postwounding (Fig. 3A) as showed by the photographs (left) and the quantitative results of wounds (right). 14*R*,21-diHDHA was as efficient as 14*S*,21-diHDHA in promoting wound closure at this dosage. In comparison with PBS control, granulation tissue deposition was more abundant in wounds treated with either 14*S*,21-diHDHA or

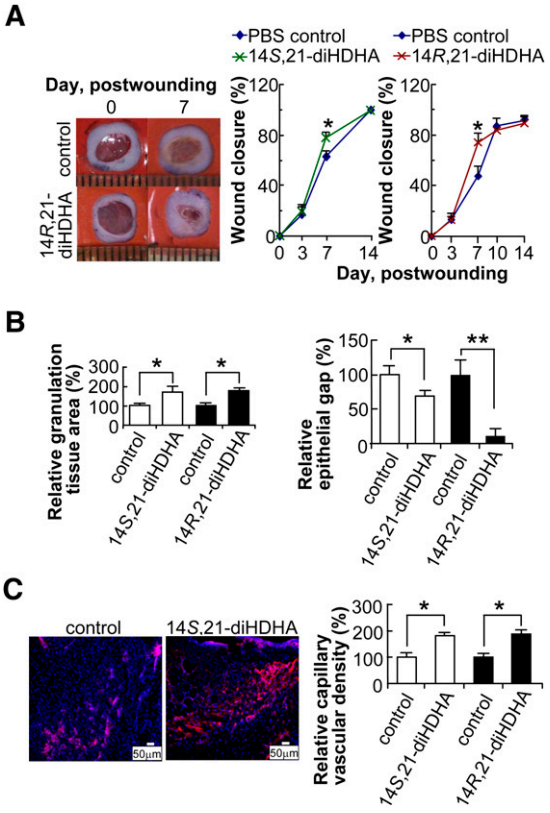

Fig. 3. 14*S*,21-diHDHAs and 14*R*,21-diHDHAs promote wound healing. Splinted excision wounding was conducted on Balb/c mice as in Fig. 1, followed by administration of 14*S*,21-diHDHA or 14*R*,21-diHDHA to wounds as detailed in "Materials and Methods." Treatment with vehicle PBS saline was the control. Results are mean ± SEM, n = 5, *$p < 0.05$ and **$p < 0.01$ as compared with the control. A: 14,21-diHDHA accelerate wound closure. Representative photographs of wounds at days 0 and 7 postwounding show wound closure (left). Wound closure (%) was measured for the treatment with 14*S*,21-diHDHA (middle) and 14*R*,21-diHDHA (right). B: 14*S*,21-diHDHA and 14*R*,21-diHDHA promotes granulation tissue formation and reepithelialization in wounds by increasing the total granulation tissue area (left) and reducing epithelial gap (right), as determined in hematoxylin-eosin stained cryosections of wounds in comparison with PBS control. C: 14*S*,21-diHDHA and 14*R*,21-diHDHA increase the capillary vascular density in wound beds. Micrographs (left) show vasculatures as CD31+ cells in wound cryosections stained with rat anti-mouse CD31 antibody then with PE-goat anti-rat IgG (red); nuclei were stained with Hoechst 33342 (blue). Capillary vascular densities were quantified (right) as CD31+ cells in wound-bed/field relative to PBS control. Cryosections were conducted on wound skin collected immediately after sacrifice of the mice at day 4 postwounding.

14*R*,21-diHDHA. 14*S*,21-diHDHA (50 ng/wound) significantly increased granulation tissue area (by >65%) (Fig. 3B, left) and reduced epithelial gaps (by >30%) (Fig. 3B, right) which was determined by hematoxylin-eosin staining of cryosections at the widest wound beds and microscopic analysis (18–20). Immunohistological staining of wound skin cryosections for endothelial protein CD31 showed increased capillary vasculature (by >80%) in 14*S*,21-diHDHA treated wounds at day 4 postwounding compared with vehicle (PBS)-treated wounds (Fig. 3C).

14*R*,21-diHDHA potently increased granulation tissue area by >65% (Fig. 3B, left), reduced epithelial gap by >90% (Fig. 3B, right), and enhanced the capillary vascular density by >80% (as CD31+ cells/microscope field) (Fig. 3C, right) at dose of 50 ng/wound.

DISCUSSION

Our results show that wounding induced formation of novel 14*S*,21*R*- and/or 14*R*,21*S*-diHDHA, 14*S*,21*S*-diHDHA, and 14*R*,21*R*-diHDHA (Fig. 1A and 1B, top). P450 transforms 14*S*-HDHA to 14*S*,21*R*-diHDHA and 14*S*,21*S*-diHDHA (Fig. 1B, upper middle), where the 12-LOX is the critical enzyme for the generation of 14*S*-HDHA from DHA (Fig. 1C, middle). P450 converts DHA to 14*R*-HDHA and 14*S*-HDHA (data not shown), and further transforms 14*R*-HDHA to 14*R*,21*S*-diHDHA and 14*R*,21*R*-diHDHA (Fig. 1B, lower middle). Although 14*R*-HDHA is a better substrate than 14*S*-HDHA to be transformed to 14,21-diHDHAs by the P450 we used (Fig. 1B, bottom), the reactivity of 14*R*-HDHA and 14*S*-HDHA to be converted to 14,21-diHDHA stereoisomers in wounds need to be further studied because profile and activities of the P450 that catalyze the conversion are not yet established.

L-12-LOX and P450 exist in Mfs (11–15). Consistent with the existence of these enzymes, Mfs produce 14*S*,21*R*-diHDHA and 14*S*,21*S*-diHDHA (Fig. 2B). Mfs are present in wound sites, participate in wound healing (1), and are likely to have 12-LOX and or P450 in wounds to produce 14*S*,21-diHDHAs and 14*R*,21-diHDHAs (**Fig. 4**). The exact amount of contribution from Mfs to 14*S/R*,21-diHDHA formation in skin wounds remains to be established and is of interest for future study. However, their contribution is likely to be significant because Mfs surge in wound sites at certain times during the course of wound healing (37, 38).

The tentative formation pathways for 14*S*,21-diHDHAs and 14*R*,21-diHDHAs are summarized as follows (Fig. 4): 14*S*-HpDHA is generated from DHA by 12-LOX and then is reduced to 14*S*-HDHA in reductive tissue environment; the 14*S*-HDHA is sequentially oxidized by P450 at the ω-1 position to 14*S*,21*R*-diHDHA and 14*S*,21*S*-diHDHA, which are similar to the ω-1 oxidation of eicosanoids catalyzed by P450 or occurred in Mfs (39, 40). Although L-12-LOX was used for the enzymatic synthesis of 14*S*-HDHA and 14*S*,21-diHDHAs, platelet-12-LOX is likely to have the same function (34). However, epidermis-12-LOX and 12*R*-LOX are likely to be inefficient in the transformation of DHA (12); P450 produces 14*R*-HDHA, 14*S*-HDHA, and 21-HDHA; then further converts 14*R*-HDHA to 14*R*,21-diHDHA, as well as 21-HDHA to 14*R*,21-diHDHA and 14*S*,21-diHDHA. It was reported that in skin P450 CYP1A1, 2B6/7, 2E1, 3A4/7, and 3A5 were detected at protein level and found to possess catalytic activities (41); and many other P450 were found in skin at mRNA level (41). CYP2E1 generates 19-HETE (16) and exists in skin; therefore, it is likely to participate in the ϖ-1 hydroxylation by converting 14-HDHA to 14,21-diHDHAs in the skin (16).

Because 14*S*,21-diHDHA and 14*R*,21-diHDHA are produced in wounds and Mfs that contribute to the healing process, as well as generated from DHA by sequential catalysis of 12-LOX and P450 that are known to contribute to vascularization and wound healing (37, 38, 42), we predicted that these endogenous small molecules are part of the effectors promoting wound healing. This was tested using the established splinted excisional wound murine model. 14*S*,21-diHDHA and 14*R*,21-diHDHA accelerate wound closure, granulation tissue formation and reepithelialization (as reduction of epithelial gap) in wounds in vivo at dose of 50 ng/wound (Fig. 3), which demonstrated their pro-healing properties (1). The dosage of 14*S*,21-diHDHA and 14*R*,21-diHDHA administered to wounds

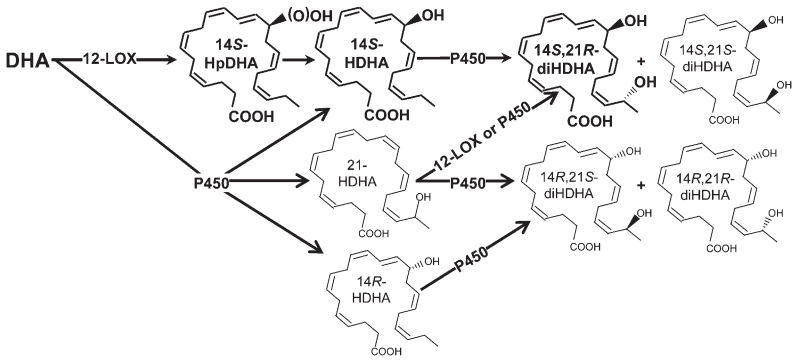

Fig. 4. Formation pathways for 14*S*,21-diHDHA and 14*R*,21-diHDHA. The main pathways are demonstrated or proposed as follows. DHA is converted by 12-LOX to 14*S*-hydroperoxy-DHA (14*S*-HpDHA), which is reduced to 14*S*-HDHA; through cytochrome P450, 14*S*-HDHA is further converted to 14*S*,21*R*-diHDHA and 14*S*,21*S*-diHDHA. Alternatively, DHA is first converted by P450 to 14*S*-HDHA, 14*R*-HDHA, and 21*S* (or *R*)-HDHA, which are further transformed by P450 to 14*R*,21*R*-diHDHA, 14*R*,21*S*-diHDHA, 14*S*,21*R*-diHDHA, and 14*S*,21*S*-diHDHA. 12-LOX and P450 exist in wounds and Mfs. The double-bond geometries of 14*S* (or *R*)-HDHA is conserved after being converted to 14,21-HDHAs on the basis of our results and reported analogous conditions for eicosanoids; this conservation also applies for the transformation of DHA to 21-HDHA. These pathways may involve novel enzymes in addition to those already recognized for eicosanoid formation.

was higher than what we could detect (less than 5 pg/mg skin) because, more than likely, the administered 14*S*,21-diHDHAs and 14*R*,21-diHDHA are only partially absorbed into the targets and because 14*S*,21-diHDHA and 14*R*,21-diHDHA also are partially degraded by metabolic enzymes before they act on targets. The study of dose-function relationship was beyond the scope of this report. Reepithelialization is one of the major processes in wound healing; moreover, it provides the basis for subsequent stages, such as fibroblast proliferation and migration and granulation tissue formation (43). Epithelial gap and granulation tissue area in histosections are parameters usually used to evaluate wound healing process (20, 43).

14*S*,21-diHDHA and 14*R*,21-diHDHA also promote vasculature formation as evidenced by increasing CD31+ cell density in cryosections of wounds (Fig. 3C). Formation of new vessels in proliferation phase is paramount to efficiently supply blood that carries nutrients, oxygen, signaling molecules, leukocytes, mesenchymal stem cells, and other cells to wounds for optimum healing. Therefore, enhancement of vascularization in wounds is an important mechanism for the promotion of wound healing by 14*S*,21-diHDHA and 14*R*,21-diHDHA. Mfs are known to play critical roles in wound healing (37, 38, 42). The Mfs produced 14*S*,21-diHDHA and 14*R*,21-diHDHA may partially represent the molecular mechanisms for macrophage pro-healing function.

In conclusion, novel 14*S*,21*R*-diHDHA and/or 14*R*,21*S*-diHDHA, 14*S*,21*S*-diHDHA, and 14*R*,21*R*-diHDHA were found in wounded skin as well as activated Mfs. The catalysis by 12-lipoxygenase and P450 in tandem or P450 alone transforms DHA to these four 14,21-diHDHA stereoisomers, suggesting novel pathways for 14,21-diHDHA formation occurring in wounds and Mfs. 14*S*,21-diHDHA and 14*R*,21-diHDHA, as novel ω-1-hydroxy docosanoid mediators, enhance wound healing. These findings provide insights into the molecular mechanisms that regulate wound healing.

The authors thank Ms. Shraddha P. Shah for excellent assistance.

REFERENCES

1. Martin, P. 1997. Wound healing–aiming for perfect skin regeneration. *Science.* **276:** 75–81.
2. Falanga, V. 2005. Wound healing and its impairment in the diabetic foot. *Lancet.* **366:** 1736–1743.
3. Serhan, C. N., R. Yang, K. Martinod, K. Kasuga, P. S. Pillai, T. F. Porter, S. F. Oh, and M. Spite. 2009. Maresins: novel macrophage mediators with potent antiinflammatory and proresolving actions. *J. Exp. Med.* **206:** 15–23.
4. Serhan, C. N., C. B. Clish, J. Brannon, S. P. Colgan, N. Chiang, and K. Gronert. 2000. Novel functional sets of lipid-derived mediators with antiinflammatory actions generated from omega-3 fatty acids via cyclooxygenase 2-nonsteroidal antiinflammatory drugs and transcellular processing. *J. Exp. Med.* **192:** 1197–1204.
5. Serhan, C. N., S. Hong, K. Gronert, S. P. Colgan, P. R. Devchand, G. Mirick, and R. L. Moussignac. 2002. Resolvins: a family of bioactive products of omega-3 fatty acid transformation circuits initiated by aspirin treatment that counter proinflammation signals. *J. Exp. Med.* **196:** 1025–1037.
6. Hong, S., K. Gronert, P. R. Devchand, R. L. Moussignac, and C. N. Serhan. 2003. Novel docosatrienes and 17S-resolvins generated from docosahexaenoic acid in murine brain, human blood, and glial cells. Autacoids in anti-inflammation. *J. Biol. Chem.* **278:** 14677–14687.
7. Marcheselli, V. L., S. Hong, W. J. Lukiw, X. H. Tian, K. Gronert, A. Musto, M. Hardy, J. M. Gimenez, N. Chiang, C. N. Serhan, et al. 2003. Novel docosanoids inhibit brain ischemia-reperfusion-mediated leukocyte infiltration and pro-inflammatory gene expression. *J. Biol. Chem.* **278:** 43807–43817.
8. Gronert, K., N. Maheshwari, N. Khan, I. R. Hassan, M. Dunn, and M. Laniado Schwartzman. 2005. A role for the mouse 12/15-lipoxygenase pathway in promoting epithelial wound healing and host defense. *J. Biol. Chem.* **280:** 15267–15278.
9. Shingel, K. I., M. P. Faure, L. Azoulay, C. Roberge, and R. J. Deckelbaum. 2008. Solid emulsion gel as a vehicle for delivery of polyunsaturated fatty acids: implications for tissue repair, dermal angiogenesis and wound healing. *J. Tissue Eng. Regen. Med.* **2:** 383–393.
10. Mezentsev, A., F. Seta, M. W. Dunn, N. Ono, J. R. Falck, and M. Laniado-Schwartzman. 2002. Eicosanoid regulation of vascular endothelial growth factor expression and angiogenesis in microvessel endothelial cells. *J. Biol. Chem.* **277:** 18670–18676.
11. Jankun, J., A. M. Aleem, S. Malgorzewicz, M. Szkudlarek, M. I. Zavodszky, D. L. Dewitt, M. Feig, S. H. Selman, and E. Skrzypczak-Jankun. 2006. Synthetic curcuminoids modulate the arachidonic acid metabolism of human platelet 12-lipoxygenase and reduce sprout formation of human endothelial cells. *Mol. Cancer Ther.* **5:** 1371–1382.
12. Siebert, M., P. Krieg, W. D. Lehmann, F. Marks, and G. Furstenberger. 2001. Enzymic characterization of epidermis-derived 12-lipoxygenase isoenzymes. *Biochem. J.* **355:** 97–104.
13. Dioszeghy, V., M. Rosas, B. H. Maskrey, C. Colmont, N. Topley, P. Chaitidis, H. Kuhn, S. A. Jones, P. R. Taylor, and V. B. O'Donnell. 2008. 12/15-Lipoxygenase regulates the inflammatory response to bacterial products in vivo. *J. Immunol.* **181:** 6514–6524.
14. Hevko, J. M., R. C. Bowers, and R. C. Murphy. 2001. Synthesis of 5-oxo-6,8,11,14-eicosatetraenoic acid and identification of novel omega-oxidized metabolites in the mouse macrophage. *J. Pharmacol. Exp. Ther.* **296:** 293–305.
15. Christmas, P., K. Tolentino, V. Primo, K. Z. Berry, R. C. Murphy, M. Chen, D. M. Lee, and R. J. Soberman. 2006. Cytochrome P-450 4F18 is the leukotriene B4 omega-1/omega-2 hydroxylase in mouse polymorphonuclear leukocytes: identification as the functional orthologue of human polymorphonuclear leukocyte CYP4F3A in the down-regulation of responses to LTB4. *J. Biol. Chem.* **281:** 7189–7196.
16. Laethem, R. M., M. Balazy, J. R. Falck, C. L. Laethem, and D. R. Koop. 1993. Formation of 19(S)-, 19(R)-, and 18(R)-hydroxyeicosatetraenoic acids by alcohol-inducible cytochrome P450 2E1. *J. Biol. Chem.* **268:** 12912–12918.
17. Han, X. 2007. An update on lipidomics: progress and application in biomarker and drug development. *Curr. Opin. Mol. Ther.* **9:** 586–591.
18. Wu, Y., L. Chen, P. G. Scott, and E. E. Tredget. 2007. Mesenchymal stem cells enhance wound healing through differentiation and angiogenesis. *Stem Cells.* **25:** 2648–2659.
19. Galiano, R. D., O. M. Tepper, C. R. Pelo, K. A. Bhatt, M. Callaghan, N. Bastidas, S. Bunting, H. G. Steinmetz, and G. C. Gurtner. 2004. Topical vascular endothelial growth factor accelerates diabetic wound healing through increased angiogenesis and by mobilizing and recruiting bone marrow-derived cells. *Am. J. Pathol.* **164:** 1935–1947.
20. Galiano, R. D., J. Michaels, M. Dobryansky, J. P. Levine, and G. C. Gurtner. 2004. Quantitative and reproducible murine model of excisional wound healing. *Wound Repair Regen.* **12:** 485–492.
21. Arendash, G. W., M. T. Jensen, N. Salem, Jr., N. Hussein, J. Cracchiolo, A. Dickson, R. Leighty, and H. Potter. 2007. A diet high in omega-3 fatty acids does not improve or protect cognitive performance in Alzheimer's transgenic mice. *Neuroscience.* **149:** 286–302.
22. Lamptey, M. S., and B. L. Walker. 1976. A possible essential role for dietary linolenic acid in the development of the young rat. *J. Nutr.* **106:** 86–93.
23. Bazan, N. G., V. L. Marcheselli, Y. Lu, S. Hong, and F. Jackson. 2008. Lipidomic approaches to neuroprotection signaling in the retinal pigment epithelium. *In* Signal Transduction in the Retina. S. J. Fliesler and O. G. Kisselev, editors. CRC Press, Boca Raton, FL. 349–374.

24. Schneider, C., Z. Yu, W. E. Boeglin, Y. Zheng, and A. R. Brash. 2007. Enantiomeric separation of hydroxy and hydroperoxy eicosanoids by chiral column chromatography. *Methods Enzymol.* **433:** 145–157.
25. Maruyama, K., J. Asai, M. Ii, T. Thorne, D. W. Losordo, and P. A. D'Amore. 2007. Decreased macrophage number and activation lead to reduced lymphatic vessel formation and contribute to impaired diabetic wound healing. *Am. J. Pathol.* **170:** 1178–1191.
26. Gronert, K., C. B. Clish, M. Romano, and C. N. Serhan. 1999. Transcellular regulation of eicosanoid biosynthesis. *Methods Mol. Biol.* **120**: 119–144.
27. Tian, H., Y. Lu, A. M. Sherwood, D. Hongqian, and S. Hong. 2009. Resolvins E1 and D1 in choroid-retinal endothelial cells and leukocytes: biosynthesis and mechanisms of anti-inflammatory actions. *Invest. Ophthalmol. Vis. Sci.* **50:** 3613–3620.
28. Lu, Y., S. Hong, R. Yang, J. Uddin, K. H. Gotlinger, N. A. Petasis, and C. N. Serhan. 2007. Identification of endogenous resolvin E1 and other lipid mediators derived from eicosapentaenoic acid via electrospray low-energy tandem mass spectrometry: spectra and fragmentation mechanisms. *Rapid Commun. Mass Spectrom.* **21:** 7–22.
29. Yin, H., L. Gao, H. H. Tai, L. J. Murphey, N. A. Porter, and J. D. Morrow. 2007. Urinary prostaglandin F2alpha is generated from the isoprostane pathway and not the cyclooxygenase in humans. *J. Biol. Chem.* **282:** 329–336.
30. Berry, K. A., P. Borgeat, J. Gosselin, L. Flamand, and R. C. Murphy. 2003. Urinary metabolites of leukotriene B4 in the human subject. *J. Biol. Chem.* **278:** 24449–24460.
31. Capdevila, J. H., V. R. Holla, and J. R. Faick. 2005. Cytochrome P450 and the metabolism and bioactivation of arachidonic acid and eicosanoids. *In* Cytochrome P450: Structure, Mechanism, and Biochemistry. 3rd edition. Paul R. Ortiz de Montellano, editor. Kluwer Academic / Plenum Publishers, New York. 531–546.
32. Hong, S., Y. Lu, R. Yang, K. H. Gotlinger, N. A. Petasis, and C. N. Serhan. 2007. Resolvin D1, protectin D1, and related docosahexaenoic acid-derived products: analysis via electrospray/low energy tandem mass spectrometry based on spectra and fragmentation mechanisms. *J. Am. Soc. Mass Spectrom.* **18:** 128–144.
33. German, J. B., G. G. Bruckner, and J. E. Kinsella. 1986. Lipoxygenase in trout gill tissue acting on arachidonic, eicosapentaenoic and docosahexaenoic acids. *Biochim. Biophys. Acta.* **875:** 12–20.
34. Kim, H. Y., J. W. Karanian, T. Shingu, and N. Salem, Jr. 1990. Stereochemical analysis of hydroxylated docosahexaenoates produced by human platelets and rat brain homogenate. *Prostaglandins.* **40:** 473–490.
35. Lagarde, M., M. Croset, M. Guichardant, and M. Dechavanne. 1985. Role of lipoxygenase products in platelet function: relation to fatty acid modified phospholipids. *Adv. Exp. Med. Biol.* **192:** 327–335.
36. VanRollins, M., R. C. Baker, H. W. Sprecher, and R. C. Murphy. 1984. Oxidation of docosahexaenoic acid by rat liver microsomes. *J. Biol. Chem.* **259:** 5776–5783.
37. Broughton II, G., J. E. Janis, and C. E. Attinger. 2006. The basic science of wound healing. *Plast. Reconstr. Surg.* **117:** 12S–34S.
38. Martin, P., and S. J. Leibovich. 2005. Inflammatory cells during wound repair: the good, the bad and the ugly. *Trends Cell Biol.* **15:** 599–607.
39. Kroetz, D. L., and D. C. Zeldin. 2002. Cytochrome P450 pathways of arachidonic acid metabolism. *Curr. Opin. Lipidol.* **13:** 273–283.
40. Oliw, E. H., F. P. Guengerich, and J. A. Oates. 1982. Oxygenation of arachidonic acid by hepatic monooxygenases. Isolation and metabolism of four epoxide intermediates. *J. Biol. Chem.* **257:** 3771–3781.
41. Swanson, H. I. 2004. Cytochrome P450 expression in human keratinocytes: an aryl hydrocarbon receptor perspective. *Chem. Biol. Interact.* **149:** 69–79.
42. Nurden, A. T., P. Nurden, M. Sanchez, I. Andia, and E. Anitua. 2008. Platelets and wound healing. *Front. Biosci.* **13:** 3532–3548.
43. Braiman-Wiksman, L., I. Solomonik, R. Spira, and T. Tennenbaum. 2007. Novel insights into wound healing sequence of events. *Toxicol. Pathol.* **35:** 767–779.